

# A Parametric Design Study for a Swashplateless Helicopter Rotor with Trailing-Edge Flaps

Jinwei Shen

Inderjit Chopra

*Graduate Research Assistant*

*Alfred Gessow Professor and Director*

Alfred Gessow Rotorcraft Center,

Department of Aerospace Engineering

University of Maryland, College Park, MD 20742

## Abstract

A numerical parametric design study is conducted for a helicopter primary control system utilizing trailing-edge flaps. The swashplateless rotor design is implemented by modifying a production modern bearingless rotor using plain flaps on the blades, and by replacing the pitch link to fixed system control system assembly with a root spring. A comprehensive rotorcraft analysis based on UMARC is carried out to obtain the results for both the swashplateless and a conventional baseline rotor configuration. The key parameters are blade pitch index angle, torsional frequency, flap location, length, chord and overhang. The predictions show that the blade pitch index angle is a key parameter in the reduction of flap deflections and actuation requirement. By lowering the blade root spring stiffness, the control effectiveness of the trailing-edge flap is increased. A flap length of  $22\%R$  with flap chord ratio of 0.30, overhang length of 15% chord, and located around  $83\%R$ , are found to generate an optimum design in terms of reducing actuation power while maintaining flap control authority. Blade aeroelastic stability predictions indicate that the swashplateless rotor is stable and has higher damping in blade lag, flap, and torsional modes when compared with a conventional rotor for most of the cases studied.

## Introduction

The pitch control device for a helicopter rotor blade was one of the great design challenges faced by the earliest rotorcraft engineers, and it remains one of the most complex, precise and flight critical devices on rotorcraft today. The rotorcraft pioneers invented essentially two means of altering blade pitch: the trailing-edge flap system and the swashplate mechanism. The Pescara (Ref. 1) helicopter of 1922 featured plain flaps for blade pitch control, whereas servo flaps, introduced by d'Ascanio (Ref. 2) around 1930, have been a feature of Kaman aircraft (Refs. 3–6) since the late 1940's. Hafner (Ref. 7), in the late 1920's, developed a swashplate mechanism, which was

---

Revised version of paper presented at the American Helicopter Society 58th Annual Forum, Montréal, Canada, June 11-13, 2002

to become the standard means of providing pitch control on modern helicopters (Ref. 8). The swashplate mechanism imposes blade pitch control directly at the blade root whereas the trailing-edge flap system provides pitch change indirectly via blade elastic twist caused by pitching moment variation with flap deflections. The swashplate mechanism is generally favored by most helicopter engineers over the trailing-edge flaps, however, it has some major drawbacks, such as numerous exposed linkages, bearings, push rods and hinges, which are maintenance intensive, inspection critical, costly and act as a significant source of drag. With the recent emergence of high energy-density smart material actuators, it appears that active trailing-edge flaps may provide an alternative for blade pitch controls (Ref. 9). Furthermore, trailing-edge flaps have also received considerable interest among rotorcraft engineers for the reduction of helicopter vibration and noise (Refs. 10–15). The use of a trailing-edge flap for primary control appears attractive in the context of an actively controlled rotor, where embedded flaps can perform multiple functions. The trailing-edge flap deflections can be accomplished either using a swashplate (as is the case with Kaman rotorcraft) or using actuators placed in the rotating frame (present case of swashplateless rotor).

There are primarily two types of flaps suitable for using on helicopter blades: servo flaps and plain flaps. The servo-flap design consists of auxiliary airfoil sections that are located aft of the trailing edge of the main blades. Despite the successful service history of servo-flaps for blade pitch control (Refs. 4, 6), they are somewhat inefficient because of the high drag resulting from exposure of the hinges and supporting structure, and reduction in aerodynamic efficiency caused by the flap hinge gap (Ref. 16). An alternative configuration, the plain flap, is the subject of the present investigation, and coupled with the use of smart materials, provides an attractive solution. In this configuration, the flap is integrated into the rotor blade by locating the flap actuation and support structure, hinge, and linkage assembly within the blade profile, thereby resulting in a reduction in aerodynamic drag, and an increase of flap effectiveness by narrowing the hinge gap. However, compared with servo flaps, plain flaps are located much closer to the blade elastic axis and hence their capability to generate pitching moments is correspondingly reduced.

A recent study, using a simple rigid rotor model, explored the feasibility of a swashplateless

rotor with plain trailing-edge flaps (Ref. 16). It was concluded that plain trailing-edge flaps have the potential to satisfy the general requirements for primary flight controls. The study (Ref. 16) also indicated that the blade fundamental torsional frequency would likely need to be lowered to 1.5 to 2.5/rev and the constraints associated with aeroelastic stability and flutter of rotor blades with such low torsional frequency should be thoroughly investigated. Lemnios, Wei and others (Refs. 4, 5) presented modeling and correlation for Kaman's SH-2 rotor, which utilizes the servo-flap type system as a primary control device. The analysis in Ref. 4 used a modified version of the rotorcraft flight simulation code C81, with airfoil data tables used to obtain the aerodynamic coefficients of the servo flap. Straub and Charles (Ref. 17) examined the preliminary requirements of the swashplateless design for an Advanced Rotor and Control System (ARCS) concept. Both a servo-flap type system and a combination of plain flap and blade root actuator mechanism were studied. The study concluded that the dual control concept is superior to the servo-flap design in maneuverability and basic performance. Virtually all of the recent numerical and experimental studies of a rotor with trailing-edge flaps focused on hub vibration minimization or rotor noise reduction relative a conventional rotor with a swashplate control system (Refs. 10–15). In a recent study, however, the authors developed a comprehensive analysis (Ref. 18) for a swashplateless rotor with trailing-edge flaps based on UMARC (University of Maryland Advanced Rotorcraft Code) (Ref. 19). A swashplateless rotor with plain flaps was shown to be trimmed successfully with a trailing-edge flap control system in the complete range of advance ratios. Furthermore, the required flap angles were found to be moderate with a proper selection of blade pitch index angle. A multicyclic controller was implemented with the swashplateless rotor analysis, in order to show that the plain flaps have the capability of performing both primary rotor control and active vibration control functions.

The objective of the present paper is to present a parametric study of various key design variables involved in the primary control with plain trailing-edge flaps and systematically examine the aeroelastic stability characteristics of such a swashplateless rotor system.

## Analytical Model

The baseline rotor used in the present study is the MD-900 Explorer, a 6000 pound commercial helicopter. The MD-900 rotor is a 5-bladed bearingless rotor with characteristics given in Table 1. The blade is attached to the hub by means of a dual load path flexbeam and torque tube assembly. The torsional loads are primarily carried through the torque tube, which is attached to the hub by an elastomeric snubber and to the control system by the pitch horn. The control system stiffness of the MD-900 rotor is 316 lb/in, which results in a blade fundamental torsional frequency of 3.03/rev. The present swashplateless rotor design modifies the baseline rotor by replacing the pitch link assembly with a linear root spring. A typical root spring stiffness used in the present study is 119 lb/in, resulting in a blade fundamental torsional frequency of 2.1/rev. The torque tube is unaltered in the swashplateless rotor design, and serves as an aerodynamic fairing, as well as providing inplane blade damping through the snubber.

The baseline rotor analysis is taken from UMARC. The modeling of the swashplateless rotor with trailing-edge flaps is discussed in Ref. 18. The following briefly outlines the analysis and solution procedure adopted. The present analysis incorporates finite element methodology in space and time. The blade is modeled as an elastic beam undergoing flap bending, lag bending, elastic twist and axial deformation. The rotor blades are discretized into a finite number of beam elements, each with fifteen degrees of freedom. The flexbeam and torque tube consist of four and three beam elements respectively. Twelve spatial elements are used to model the main blade and one element to model the swept tip. Eight time elements with sixth order shape functions are used to calculate the coupled trim solution. The trailing-edge flap motion is prescribed, and dynamics of flap actuator system is neglected for this study (Ref. 14). Flap inertial effects are included both in the formulation of the blade equations of motion and the hub loads computation. The coupled blade response and the trim control settings are solved simultaneously for a wind tunnel trim condition.

In order to reduce actuation power, trailing-edge flap aerodynamic balance (nose overhang) (Ref. 20) was incorporated to alter the aerodynamic characteristics of the airfoil/flap. Flap nose overhang is defined as the hinge offset from the leading-edge of the flap in terms of the

full chord of the airfoil (Fig. 1). A typical overhang value places the flap hinge at 10% chord from the leading edge of the flap. For a 35% chord flap, this translates into an overhang of approximately 29% of the flap chord. To model the aerodynamically balanced flap, a quasi-steady model adapted from Theodorsen's theory (Ref. 21) is used. This model considers the gap sealed; that is, no leak of fluid between the flap and the base airfoil. The Drees linear inflow is used to obtain the induced inflow distribution over the rotor disk.

## **Analysis of Swashplateless Rotor**

Deflection of a trailing edge flap alters the camber of the blade section and results in a change in pitching moment. That change in pitching moment causes the blades to pitch against the root spring to establish aerodynamic equilibrium. The trim variables for a swashplateless rotor are flap collective deflection,  $\delta_0$ , and flap cyclic deflections,  $\delta_{1c}$  and  $\delta_{1s}$ .

Two unique characteristics of swashplateless rotor, compared with a conventional rotor, are torsionally soft blades and pre-collective angles. Torsionally soft blades, which can be achieved using soft root springs, are required to increase the flap effectiveness (the ratio of blade pitch to trailing-edge flap deflection angle). Pre-collective pitch angle or indexing (Figure 2) is used to reduce the amount of blade pitch travel excited by the trailing-edge flap, and hence decrease the required flap deflections. The pre-collective pitch defines the three-quarter radius blade pitch value relative to the hub plane. Pitch index angle is normally selected to be higher than is required to trim the helicopter at a selected forward speed, i.e. the cruising speed. As the rotor is accelerated to its normal rotational speed, the nose-down pitching moment generated by the flaps and the baseline blade airfoil will twist the blade nose-down to the desired pitch position. Higher index angle requires downward deflected flap, which generates upward lift on the blade. This upload moves the blade airload distribution inboard, and improves the rotor performance in hover and forward flight conditions (Ref. 6).

For a swashplateless rotor with flaps, the control angle input to the blade is given by:

$$\delta(\psi) = \delta_0 + \delta_{1c}\cos(\psi) + \delta_{1s}\sin(\psi) \quad (1)$$

and the blade pitch angle consists of the blade index angle and the elastic twist induced by flap control inputs;

$$\theta(\psi) = \theta_{index} + \phi_{twist}(\psi) \quad (2)$$

The flap control angles are obtained from the coupled trim procedure. Given a set of controls, shaft orientation, and inflow distribution, the coupled analysis determines the blade response, and provides the blade loads together with the fixed system hub loads. In turn, these loads and responses are used in a separate set of equations representing either the vehicle free-flight equilibrium, or a prescribed wind tunnel operating condition. These equations govern the rotor control settings. A typical wind tunnel experimental procedure involves adjusting the controls to achieve zero first harmonic blade flapping, with a prescribed thrust level ( $C_T/\sigma = 0.075$ ) and shaft angles (Table 2). The trim solution and blade responses are updated iteratively until the convergence criteria are reached. The incremental lift and pitching moment of an active trailing-edge flap, consisting of both inertial and aerodynamic contributions, are included in this coupled trim procedure.

## **Aeroelastic Stability**

Because the swashplateless rotor design demands an unconventional torsionally soft blade system (Ref. 16), such a rotor can be susceptible to aeroelastic instabilities. Aeroelastic stability of a rotor with trailing-edge flaps was thoroughly studied in Ref. 14. This analysis was extended to provide aeroelastic stability predictions for a swashplateless rotor. The coupled blade equations of motion were linearized by using small perturbations about a steady trimmed solution. Stability was then determined from an eigenanalysis of the homogeneous equations. Because the trailing-edge

flap motion is prescribed in this study, the stability of the trailing-edge flap mode is not included.

## Actuation Power

The actuation power of the flap system is calculated by integrating the product of the hinge moment and flap deflection rate over one complete rotor revolution. Although the instantaneous power required at the flap hinge may be negative over some portions of the azimuth, it is assumed that the actuator is unable to transfer the power back to its power supply, so that the negative power is neglected. Therefore, the actuation power of the flap system is:

$$P_f = \frac{N_b}{2\pi} \int_0^{2\pi} \max(-M_h \dot{\delta}, 0) d\psi \quad (3)$$

where  $N_b$  is number of blades,  $M_h$  is flap hinge moment and  $\dot{\delta}$  is flap velocity. The actuation power presented in equation 3 is “ideal” because it only includes the energy used to drive the flap system, and neglects the heat dissipation of the smart actuators.

## Results and Discussion

The selected baseline rotor configuration for the swashplateless system is a modified version of the MD-900 rotor, with a root pitch link stiffness of 119 lb/in and pitch index angle of 18°. The baseline trailing-edge flap characteristics are given in Table 1. Trailing-edge motion is positive for downward deflection, and hinge moment is positive when its direction is “nose-up” (and “tail-down”).

### Baseline Swashplateless Rotor

Figure 3 compares conventional and swashplateless rotor control settings for the complete range of advance ratios ( $\mu = 0$  to 0.35). For comparison purposes, the conventional rotor used in this

section has the same torsional frequency as the swashplateless rotor configuration. Figure 3(a) presents the trailing-edge flap deflection required to trim the swashplateless rotor. The blade index angle used in the simulation is  $18^\circ$ , which yields small collective flap at an advance ratio of 0.3. The required half peak-to-peak values of trailing-edge flap deflections are shown to be below  $4^\circ$ , and the mean values are smaller than  $6^\circ$  in the complete range of advance ratios. The trailing-edge flap collective angle,  $\delta_0$ , is deflected downward at advance ratios below 0.30 to bring the blade pitch down, whereas  $\delta_0$  is deflected upward at an advance ratio of 0.35 to further twist the blade nose-up to the desired position. The longitudinal cyclic,  $\delta_{1s}$ , shows small variation at advance ratios below 0.30, and increases rapidly at advance ratios above 0.30. This is because of the cyclic twist effect from the flap collective angle,  $\delta_0$ , in forward flight; that is, flap collective generates a cyclically varying pitching moment because of the laterally asymmetric air velocities. This results in a cyclic blade pitch variation from flap collective deflection. The cyclic blade pitch of a downward deflected flap collective,  $\delta_0$ , benefits flap longitudinal cyclic,  $\delta_{1s}$  whereas, upward,  $\delta_0$  is against  $\delta_{1s}$ . Trailing-edge flap lateral cyclic,  $\delta_{1c}$ , is generally small because of the small blade lateral cyclic pitch. Figure 3(b) compares the 75%R pitch angles of a conventional and swashplateless rotor. The pitch angle is relative to hub plane; that is, the pitch index angle is included for the swashplateless rotor. The collective blade pitch of the swashplateless rotor exhibits smaller  $\theta_0$  than the conventional rotor at advance ratios below 0.30. This is because of the favorable additional lift generated from the downward deflected trailing-edge flaps. The blade longitudinal and lateral cyclic pitch of the swashplateless rotor exhibits similar trends to those of the conventional rotor, with the small difference attributable to the additional lift generated by the flap cyclic deflections,  $\delta_{1s}$  and  $\delta_{1c}$ . Figure 3(c) illustrates flap actuation requirements at several advance ratios. By using flap aerodynamic balance overhang, the hinge moments are relatively small in the complete range of advance ratios. The actuation power is dominated by the flap deflection amplitude and hinge moment. At an advance ratio of 0.30, the actuation power is a minimum, because the trailing-edge flap cyclic angles are small (as shown in Fig. 3(a)).

## Blade Pitch and Elastic Twist

The mechanism of primary control with trailing-edge flaps involves the entire blade pitch motion about the root spring and blade sectional elastic twist about the elastic axis. It is apparent that the root spring stiffness and blade torsional stiffness distribution are important design parameters. Figure 4 presents the variation of blade fundamental torsional frequency with root spring stiffness and blade torsional stiffness distribution. The blade torsional stiffness is changed as a percentage of baseline blade value. As may be expected, the blade torsion frequency exhibits an increase with root spring stiffness as well as with torsional stiffness, though it shows a greater sensitivity to root spring stiffness. Figure 5 illustrates the effects of root spring and blade torsional stiffness on blade pitch and elastic twist. The predictions for a conventional MD-900 are shown for reference. Three swashplateless rotor configurations are shown: first, the baseline rotor with a torsion frequency of 2.1/rev, second swashplateless rotor with soft root spring (69 lb/in) with a torsional frequency of 1.8/rev and last a swashplateless rotor with 50% reduced blade torsional stiffness with a torsion frequency of 2.04/rev. Figure 5(a) illustrates the variation of blade elastic twist with blade station at an azimuth angle of zero degree. The blade segments extend from approximately  $21\%R$  to the tip and the flexbeam and torque tube connect the root of the blade to the hub. As may be expected, the blade with soft torsional stiffness exhibits a larger twist variation than the baseline blade. Figure 5(b) presents the variation of blade tip pitch for one complete rotor revolution at an advance ratio of 0.3. The tip pitch of the swashplateless rotors exhibit the 1/rev characteristics of primary control function, and shows small difference between the baseline swashplateless configuration and soft root spring case or soft torsional stiffness case. The difference is primarily a result of the required trim setting that slightly changes as the blade properties vary.

Figures 6, 7 and 8 respectively show the effect of blade pitch index angle, blade root spring stiffness and blade torsional stiffness distribution on the flap angle, blade pitch and flap actuation requirement.

## Blade Pitch Index Angle

Figure 6(a) shows that the mean values of flap deflection,  $\delta_0$ , are decreased, because the required blade collective pitch motion is reduced with higher index angle. The flap collective deflection reaches almost zero with a pitch index angle of  $16^\circ$  at an advance ratio of 0.3, and increases thereafter, because the index angle provides more pitch than is needed for steady flight trim (i.e. downward flap deflections would be required). The flap cyclic deflections reduce because of the favorable blade cyclic twist effect induced by downward flap collective deflection,  $\delta_0$ , in the asymmetric aerodynamic environment. Figure 6(b) shows that blade collective pitch decreases with blade index angle because of the additional lift generated by a downward deflected flap. Similarly, the lift obtained by cyclic flap inputs alters the blade longitudinal cyclic pitch. Figure 6(c) shows the half peak-to-peak value of flap hinge moment changes less because of small variation of cyclic components of blade pitch angle and flap deflections. The mean values vary from a nose-up hinge moment at zero index angle, to a nose-down moment for an index angle below  $8^\circ$ . The actuation power decrease with larger index angles because of the reduction of flap cyclic deflection and hinge moment. Figure 6 suggests an optimal blade pitch index angle of  $18^\circ$  for an advance ratio of 0.3 with the baseline root spring. However, the optimal pitch index angle is varying with advance ratio because of the variation of required blade pitch, and as a result, a compromise is required.

## Blade Root Spring Stiffness

Figure 7 investigates the effect of root spring stiffness on flap deflection, blade pitch, and actuation requirement. Figure 7(a) shows the flap collective deflection increases dramatically with increasing blade root spring. Flap collective deflection also changes from upward deflection for root spring stiffness at 69 lb/in to downward deflection for the rest cases. This is because the pitching down aerodynamic moment generated by the baseline blade is also more effective in driving the blade pitch nose-down with a softer root spring. This results in the flap deflecting upward to pitch up the blade, to achieve the required trim position. Flap cyclic deflections increase after root spring

stiffness of 150 lb/in, and it also shows the cyclic effects of flap collective. When flap collective is upward, larger cyclic is required. Figure 7(b) compares blade pitch angle of swashplateless and conventional rotor with different root spring stiffness. For the conventional rotor, the root spring stiffness represents the value of rotor control system stiffness. The blade collective pitch of the swashplateless rotor reduces with increasing spring stiffness because of the favorable lift generated by the flap downward deflections. The blade cyclic pitch also exhibits a variation with root spring stiffness because of the lift generated by the cyclic flap deflections. Figure 7(c) shows mean of the hinge moment is directly related to the corresponding components of the flap collective, increasing with increasing root spring stiffness. The actuation power shows a minimum at root spring of 119 lb/in, which has small cyclic flap deflection, and increases thereafter. Figure 7 shows that flap deflections, both collective and cyclic, are small using a root spring around 119 lb/in, which results in a blade torsional frequency of 2.1/rev. However, the selection of low root spring stiffness should be considered along with targeted forward speed and selection of index angle. The selection of soft root spring can be of concern to aeroelastic stability and has been examined carefully.

## **Blade Torsional Stiffness Distribution**

Figure 8(a) shows that flap collective increases with increasing blade torsional stiffness. This increase is attributable to the reduction in twist motion along the blade segment. The blade torsion stiffness parameter was found to be less effective at raising the flap effectiveness, because the trailing-edge flap achieves primary control mainly through blade pitch at the root spring, rather than blade sectional twist motion. Figure 8(b) shows a small variation of blade pitch angle with torsional stiffness. This is because the small changes in flap angle result in a minimal increment of lift through the plain flap motion. Figure 8(c) shows a relatively small change in both hinge moment and actuation power with blade torsional stiffness. Figure 8 shows the torsionally soft blade as the optimum design. However, the selection of blade torsional stiffness can have significant influence on rotor performance and dynamics.

## Flap Spanwise Location

Flap spanwise location was identified as an important parameter in several studies of flaps used for active vibration control (Refs. 10, 11, 13). Figure 9(a) shows a reduction in both collective and cyclic flap deflection being achieved by moving the flap spanwise location toward the blade tip. This is because the flap effectiveness increases when the flap is located near the blade tip, where high dynamic pressure exists. Figure. 9(b) shows that the mean and half peak-to-peak components of hinge moment exhibit a very small variation with the flap location because of two counteracting effects when moving flap outboard: the raising of dynamic pressure, and the reduction of flap deflections. For a given baseline flap length of  $18\%R$ , Figure 9 suggests the optimum flap location at  $83\%R$  because moving flap further outboard achieves small reduction on flap deflection and actuation requirement.

## Flap Length

Both flap collective and cyclic reduce with increasing flap length, as shown in Figure 10(a), because flap effectiveness increases. Figure 10(b) shows the effect of flap length on actuation requirement. Although both cyclic and collective flap deflections become small with increasing flap length, the mean and half peak-to-peak components of the hinge moment increase. Overall, actuation power decreases slightly with increasing flap length. Considering both the flap effectiveness and actuation requirement, Figure 10 suggests an optimal flap length of  $22\%R$ . Further increasing the flap length achieves only small reductions in flap deflections and actuation requirements.

## Flap Chord Ratio

The flap chord ratio is a key design parameter, because it plays an important role in determining the dominant flap effect (i.e. incremental lift or pitching moment). Previous test data and theoretical predictions related to fixed-wing trailing-edge flaps (Refs. 21, 22) show that the flap pitching moment coefficient reaches a maximum around a flap chord ratio of 0.26 without overhang, or

0.36 with overhang of 29% flap chord (Figure 11). Figure 12(a) shows that flap collective presents the minimum at 30% airfoil chord although the variation of flap collective and cyclic with flap chord ratio is small. This is because of the small changes of  $dc_m/d\delta$  in the range of 0.1 to 0.5c for a flap with overhang length of 29% flap chord (Fig. 11). Figure 12(b) shows both the mean and half peak-to-peak values of flap hinge moment increase with increasing flap chord ratio, which mainly results from flap hinge moment coefficient increase. The actuation power increases with flap chord ratio. Figure 12 suggests a flap chord ratio of 0.30 or smaller, when considering both flap effectiveness and actuation requirements.

## **Flap Overhang**

Figure 13(a) shows both collective and cyclic flap deflections reduce with increasing flap overhang because of the increased sensitivities to pitching moment,  $dc_m/d\delta$  (Fig. 11). Figure 13(b) shows both the mean and half peak-to-peak components of hinge moment reduce with increasing flap overhang, reaching minimum around 15% chord, and then increase thereafter. Actuation power has a minimum at a flap overhang of 15% chord. The implementation of flap overhang can be of concern to aeroelastic stability if flap overhang becomes too large (Ref. 14).

## **Aeroelastic Stability of Swashplateless Rotor**

Figure 14 presents the variation of blade stability with airspeed for both a swashplateless rotor and conventional rotor. The stability results presented are damping ratios in the rotating frame. For comparison purposes, the conventional rotor used in this section, again, has the same torsional frequency as the swashplateless rotor, i.e. 2.1/rev. Figure 14(a) compares the blade lag mode damping ratio. The behavior of the blade lag mode is important for the aeroelastic stability of the rotor system, because the coupling of this mode with the inplane hub motions, which can cause dynamic instabilities known as ground and air resonance. The swashplateless concept has higher lag damping than the conventional rotor at advance ratios below 0.325. Figure 14(b) illustrates the variation of the blade flap mode damping with airspeed, for both the swashplateless and

conventional rotor. The blade flap mode is generally a less important mode in rotor aeroelastic stability, because this mode is always adequately damped by the aerodynamic forces. Figure 14(c) compares the torsion mode damping of swashplateless and conventional rotors. Both have a well damped torsion mode, with the swashplateless rotor having a higher damping ratio than the conventional rotor at advance ratios above 0.15.

Low blade torsional frequency, which is inherent in the swashplateless design, has been known to be the cause of aeroelastic instability and flutter of the rotor blades (Ref. 23). Figure 15 presents the variation of blade aeroelastic stability with blade fundamental torsional frequency at an advance ratio of 0.3. This sweep of blade torsional frequencies was carried out by altering the blade root spring stiffness for the swashplateless concept and changing the pitch link stiffness for the conventional case. Figure 15(a) shows that blade lag mode damping of the swashplateless rotor exhibits small variation with torsional frequency, whereas the conventional rotor lag damping reduces slightly with increasing blade torsional frequency. Figure 15(b) shows that the swashplateless rotor flap damping is higher than for conventional rotor. Figure 15(c) shows that both the swashplateless and conventional rotors have moderately well damped torsional modes. The swashplateless concept has a larger torsional damping value than the conventional rotor.

## Conclusions

A parametric design study was numerically conducted for a helicopter primary control system utilizing trailing-edge flaps. The swashplateless rotor design is based on a typical production helicopter rotor, with plain trailing-edge flaps as primary control devices. The primary design parameters are summarized below:

1. The blade pitch index angle was found to be a key parameter in the design of a swashplateless rotor with trailing-edge flaps. An optimal pitch index angle will reduce both the cyclic and mean components of flap deflections, and as a result, minimize the actuation power. The

optimal pitch index angle varies with advance ratio, therefore a compromise needs to be made for the complete range of flight speed.

2. Blade root spring stiffness is another important parameter that can be used to increase the trailing-edge flap control effectiveness. It is shown that increasing blade root spring stiffness results in an increase in the magnitude of both the mean and cyclic components of the required flap deflections, and hence the actuation requirement. The present study suggests low root spring stiffness that results in a blade torsional frequency of 2.1/rev as the optimum value at an advance ratio of 0.30 and index angle of  $18^\circ$ .
3. Low blade torsional stiffness increases flap effectiveness. However, the blade torsion stiffness is less effective than blade root stiffness because the trailing-edge flap achieves primary control mainly through blade pitch at the root spring, rather than blade sectional twist motion.
4. Locating trailing-edge flaps close to the blade tip where high dynamic pressure exists, will decrease flap deflection and actuation requirement.
5. Increasing the spanwise length of the flap will increase the flap effectiveness in providing primary control. It will also reduce actuation power by lowering the required flap deflection.
6. Flap chord ratio is a key parameter in plain flap design, because it plays an important role in determining the dominant flap effect. The study suggests a flap chord ratio of around 0.30 for a flap with overhang of 29% flap chord.
7. Implementation of flap aerodynamic balance (nose overhang) is important to reduce actuation requirement. The study suggests a flap overhang of 15% chord which for a 35% chord flap translates into an overhang of approximately 43% of the flap chord.
8. The swashplateless rotor exhibits larger damping in the blade flap and torsion modes than a conventional rotor at advance ratios above 0.15. The swashplateless rotor shows larger lag

damping than the conventional at advance ratios below 0.325. A similar result was observed with the variation of blade stability with torsion frequency. Overall, the swashplateless rotor was more damped than the conventional rotor.

The results of this investigation are entirely computation, hence must be verified by appropriate tests.

## Acknowledgments

The authors gratefully acknowledge Dr. Friedrich Straub (Boeing-Mesa) for providing valuable advice and assistance. We appreciate useful additional comments from Dr. Wayne Johnson (NASA Ames). This work was supported by the Army Research Office under grant DAAD190110790 with Dr. Gary Anderson as technical monitor.

## References

<sup>1</sup>Pescara, R. P. “Screw Propeller of Helicopter Flying Machines,”. U.S. Patent 1,449,129, March 20, 1923.

<sup>2</sup>d’Ascanio, C. U.S. Patent 1,960,141, May 1934.

<sup>3</sup>Kaman, C. “Aircraft of rotary wing type,”. U.S. Patent 2,455,866, December 1948.

<sup>4</sup>Wei, F.-S. and Jones, R., “Correlation and Analysis for SH-2F 101 Rotor,” *Journal of Aircraft*, Vol. 25, (7):647–652, July 1988.

<sup>5</sup>Lemnios, A. Z. and Jones, R. “The Servo Flap – An Advanced Rotor Control System,”. In *Proceedings of AHS and NASA Ames Research Center Vertical Lift Aircraft Design Conference*, San Francisco, CA, January, 17-19 1990.

<sup>6</sup>Wei, F.-S. J. and Gallagher, F. “Servo-Flap Rotor Performance Flight Testing and Data Identification,”. In *American Helicopter Society 57th Annual Forum Proceedings*, pages 596–603, Washington, D.C., May 9-11 2001.

<sup>7</sup>Hobbs, J., *Bristol Helicopters: A Tribute to Raoul Hafner*, Frenchay Publications, Bristol, UK, 1984.

<sup>8</sup>Leishman, J. G. *Principles of Helicopter Aerodynamics*, chapter 1, Introduction: A History of Helicopter Flight. Cambridge University Press, 2000.

<sup>9</sup>Chopra, I., “Status of Application of Smart Structures Technology to Rotorcraft Systems,” *Journal of the American Helicopter Society*, Vol. 45, (4):228–252, October 2000.

<sup>10</sup>Millott, T. and Friedmann, P. “Vibration Reduction in Helicopter Rotors Using an Actively Controlled Partial Span Trailing Edge Flap Located on the Blades,” Technical Report CR 4611, NASA, June 1994.

<sup>11</sup>Milgram, J., Chopra, I., and Straub, F., “Rotors with Trailing Edge Flaps: Analysis and Comparison with Experimental Data,” *Journal of the American Helicopter Society*, Vol. 43, (4):319–332, October 1998.

<sup>12</sup>Koratkar, N. A. and Chopra, I., “Wind Tunnel Testing of a Mach-Scaled Rotor Model with Trailing-Edge Flaps,” *Journal of the American Helicopter Society*, Vol. 47, (4):263–272, October 2002.

<sup>13</sup>Shen, J. and Chopra, I. “Aeroelastic Modeling of Trailing-Edge Flaps with Smart Material Actuators,”. In *Proceedings of the 41<sup>st</sup> AIAA/ASME/ASCE/AHS/ASC structure, structural dynamics, and materials conference*, AIAA-2000-1622, page 14, Atlanta, GA, April, 3-6 2000.

<sup>14</sup>Shen, J. and Chopra, I. “Aeroelastic Stability of Smart Trailing-Edge Flap Helicopter Rotors,”. In *Proceedings of the 42<sup>nd</sup> AIAA/ASME/ASCE/AHS/ASC structure, structural dynamics, and materials conference*, AIAA-2001-1675, page 11, Seattle, WA, April, 16-19 2001.

<sup>15</sup>Straub, F. K. and Charles, B. D., “Aeroelastic Analysis of Rotors with Trailing Edge Flaps Using Comprehensive Codes,” *Journal of the American Helicopter Society*, Vol. 46, (3):192–199, July 2001.

<sup>16</sup>Ormiston, R. A. “Aeroelastic Considerations for Rotorcraft Primary Control with On-Blade Elevons,”. In *American Helicopter Society 57th Annual Forum Proceedings*, Washington, D.C., May 9-11 2001.

<sup>17</sup>Straub, F. and Charles, B. “Preliminary Assessment of Advanced Rotor/Control System Concepts (ARCS),” Technical Report 90-D03, USA AVSCOM, 1990.

<sup>18</sup>Shen, J. and Chopra, I. “Actuation Requirements for a Swashplateless Helicopter Control System With Trailing-Edge Flaps,”. In *Proceeding of the 43rd AIAA/ASME/ASCE/AHS structures, structural dynamics, and materials conference and 10th AIAA/ASME/AHS adaptive structures conference*, number AIAA-2002-1444, page 11, Denver, Colorado, April 2002.

<sup>19</sup>Bir, G. and Chopra, I. “University of Maryland Advanced Rotor Code (UMARC) Theory Manual,” Technical Report UM-AERO 94-18, Center for Rotorcraft Education and Research, University of Maryland, College Park, July 1994.

<sup>20</sup>Hassan, A. A., Straub, F. K., and Noonan, K. W. “Experimental/Numerical Evaluation of Integral Trailing Edge Flaps for Helicopter Rotor Applications,”. In *American Helicopter Society 56th Annual Forum Proceedings*, pages 84–102, Virginia beach, VA, May 2-4 2000.

<sup>21</sup>Theodorsen, T. and Garrick, I. E. “Nonstationary Flow about a Wing-Aileron-Tab Combination Including Aerodynamic Balance,” Technical Report No. 736, NACA, 1942.

<sup>22</sup>Hoerner, S. F. and Borst, H. V. *Fluid-Dynamic Lift*, chapter Characteristics of Airplane Control Surfaces, pages 9–1–9–30. Hoerner fluid dynamics, Bakersfield, CA, 1975.

<sup>23</sup>Chopra, I., “Perspectives in Aeromechanical Stability of Helicopter Rotors,” *Vertica*, Vol. 14, (4):457–508, 1990.

Table 1: Baseline Rotor (MD-900) and Flap Properties

<u>MD900 Rotor Data</u>	
Rotor Type	bearingless
Number of Blades	5
Rotor Diameter	34 ft.
Rotor Speed	392 RPM
Chord	$0.0492R$
Linear Twist Angle	$-10^\circ$
Solidity	0.078
<u>Trailing-Edge Flap Data</u>	
Flap Type	Plain Flap
Spanwise Length	36 inch (0.18R)
Chordwise Size	35 % (Blade Chord)
Flap Midspan Location	0.83R
Flap Hinge Overhang	10% (Airfoil Chord)

Table 2: Prescribed shaft angles in different forward speeds. (Positive is tilt forward)

Advance Ratio	Shaft Angle
$\mu$	$\alpha_s$ (deg.)
0	0
0.05	0.5
0.10	1.1
0.15	2.6
0.20	4.9
0.25	6.9
0.30	8.8
0.35	10.9

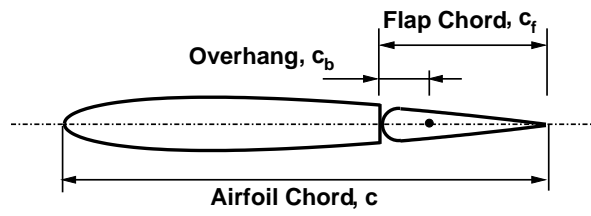


Figure 1: Trailing-edge flap with aerodynamic balance (nose overhang)

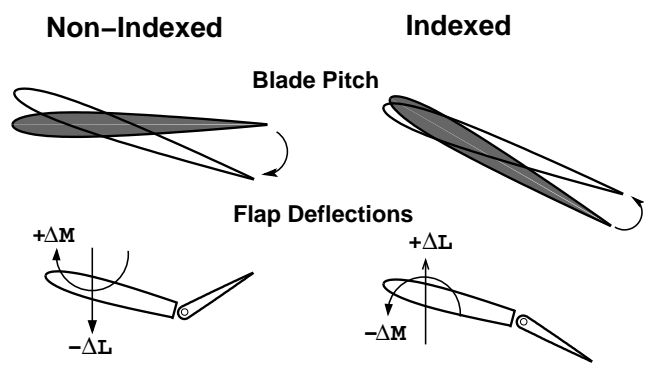
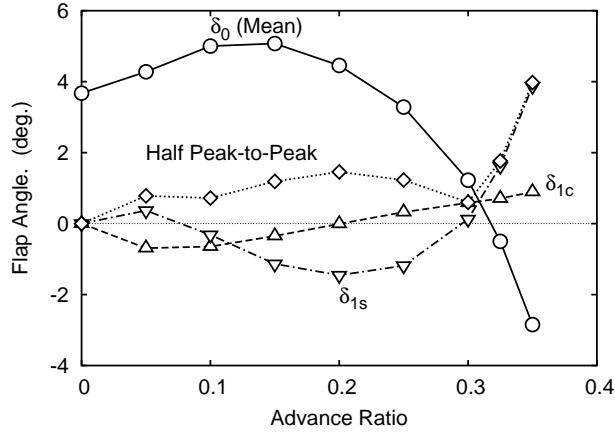
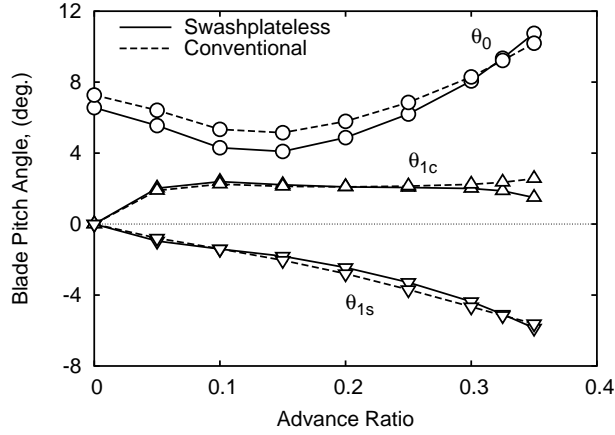


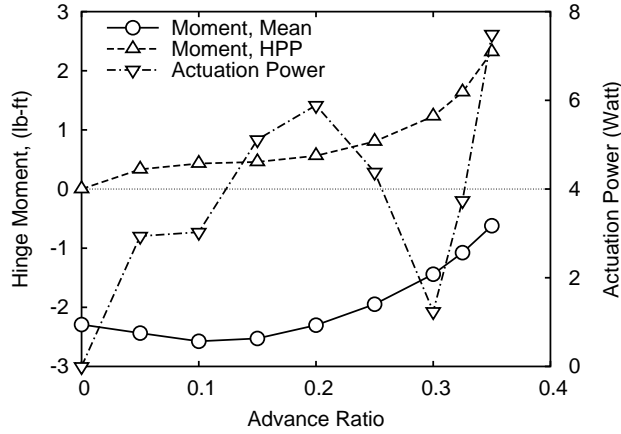
Figure 2: Blade pitch indexing



(a) Trailing-edge flap angle



(b) Blade pitch angle at 75%R



(c) Flap hinge moment and actuation power

Figure 3: Trailing-edge flap deflection, blade pitch angle, and actuation requirement of swashplateless rotor at different forward speeds (blade pitch index angle of  $18^\circ$ ,  $C_T/\sigma = 0.075$ ,  $\nu_\theta = 2.1/rev$ ). HPP: Half Peak-to-Peak

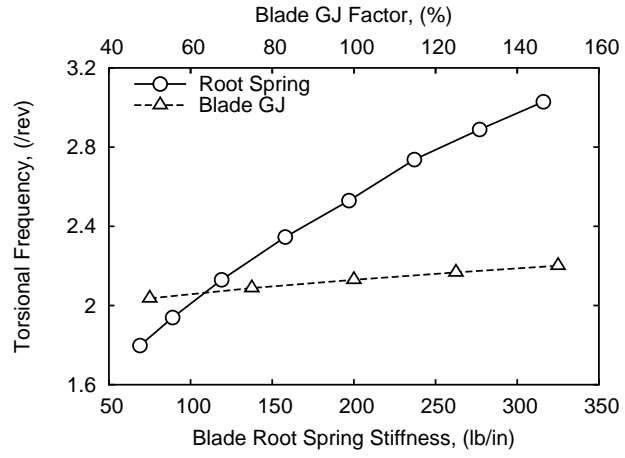
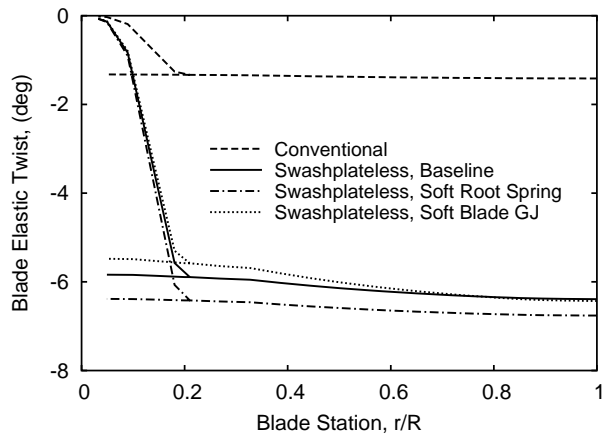
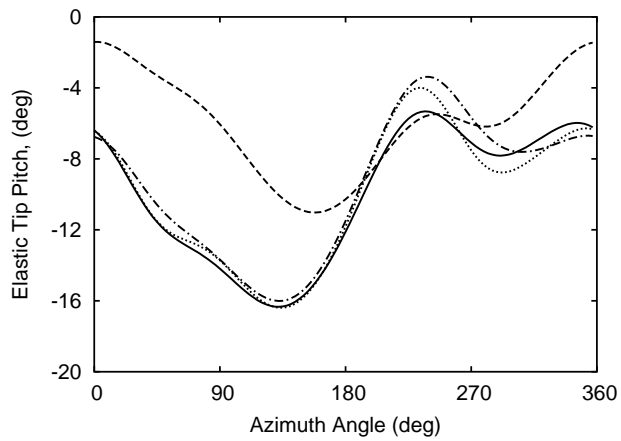


Figure 4: Variation of blade torsion frequency with root spring stiffness and blade torsional stiffness distribution.

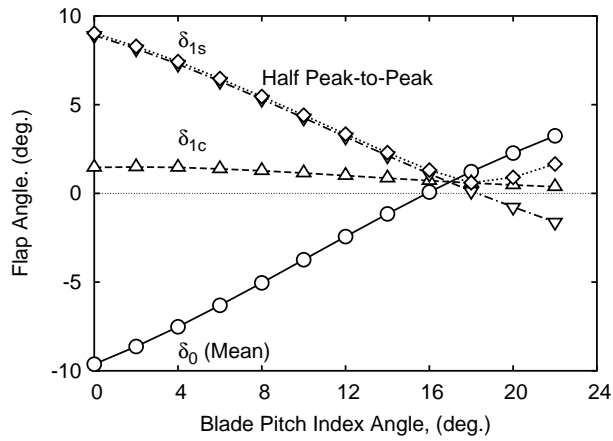


(a) Variation of blade elastic twist with blade station ( $\psi = 0^\circ$ ).

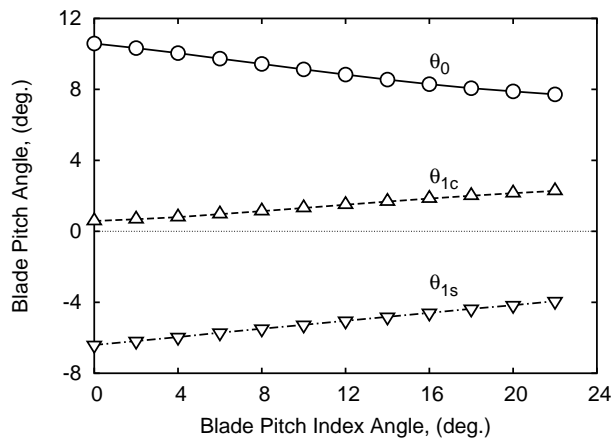


(b) Variation of blade tip pitch with azimuth angle.

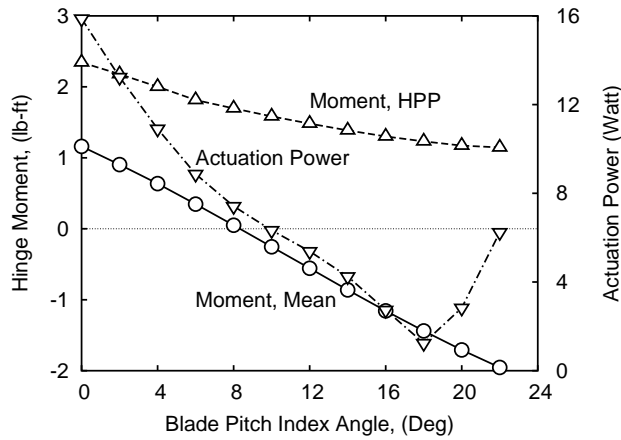
Figure 5: Effect of blade root spring stiffness and blade torsional stiffness on blade pitch and twist ( $\mu = 0.30$ ).



(a) Trailing-edge flap angle

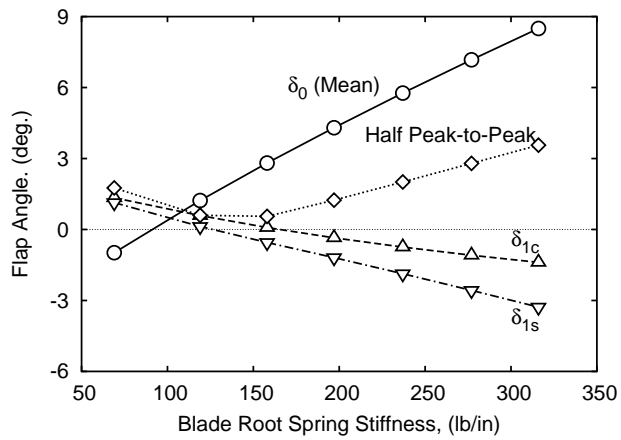


(b) Blade pitch angle at 75%R

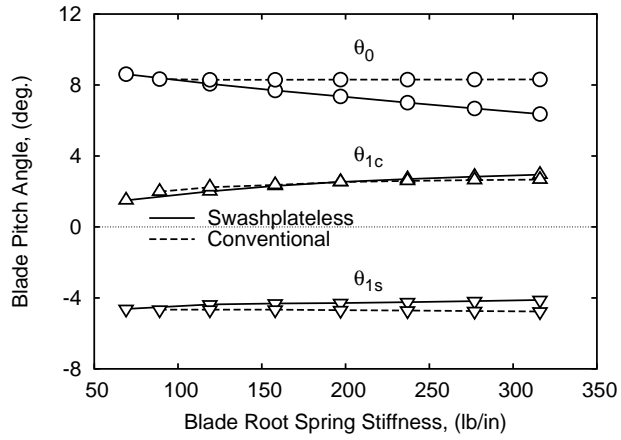


(c) Flap hinge moment and actuation power

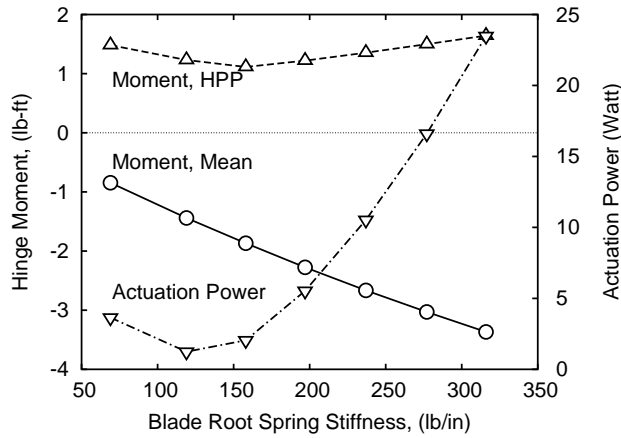
Figure 6: Effect of blade index angle on flap deflection, blade pitch angle, and flap actuation requirement ( $\nu_\theta = 2.1/rev$ ,  $\mu = 0.30$ ). HPP: Half Peak-to-Peak



(a) Trailing-edge flap angle

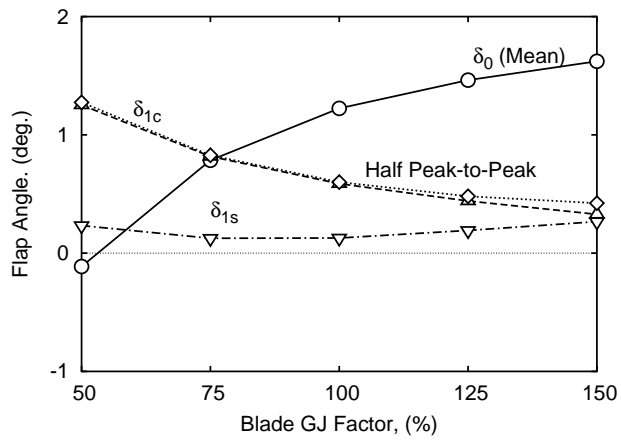


(b) Blade pitch angle at 75%R

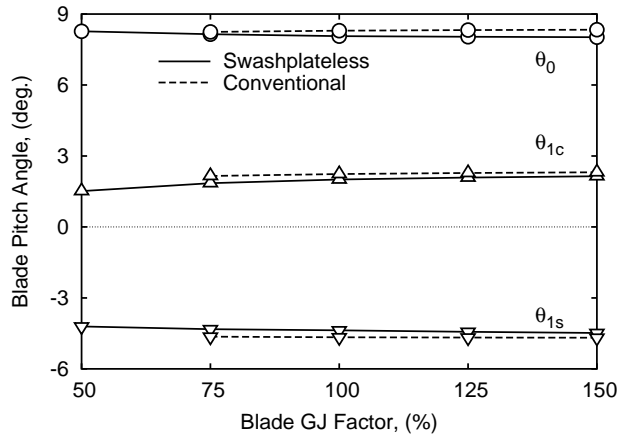


(c) Flap hinge moment and actuation power

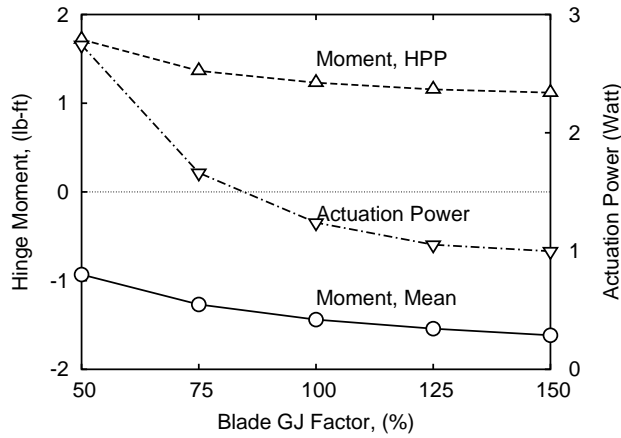
Figure 7: Effect of blade root spring stiffness on flap deflection, blade pitch angle, and flap actuation requirement (baseline blade torsional stiffness distribution, blade index angle of  $18^\circ$ ,  $\mu = 0.30$ ).



(a) Trailing-edge flap angle

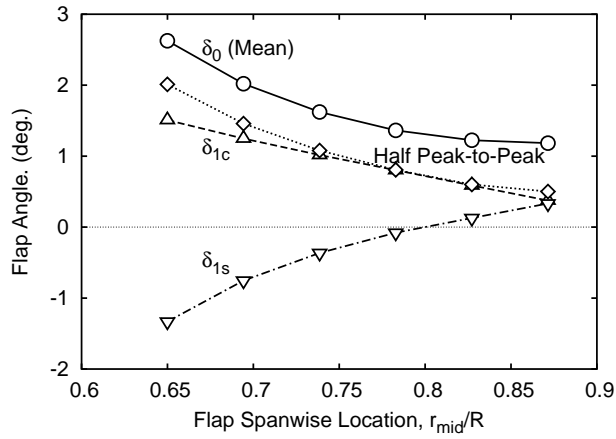


(b) Blade pitch angle at 75%R

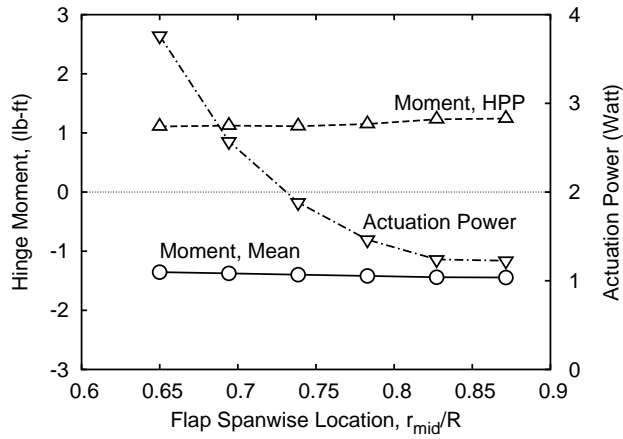


(c) Flap hinge moment and actuation power

Figure 8: Effect of blade torsional stiffness distribution on flap deflection, blade pitch angle, and flap actuation requirement (blade root spring stiffness of 119 lb/in, blade pitch index angle of  $18^\circ$ ,  $\mu = 0.30$ ).

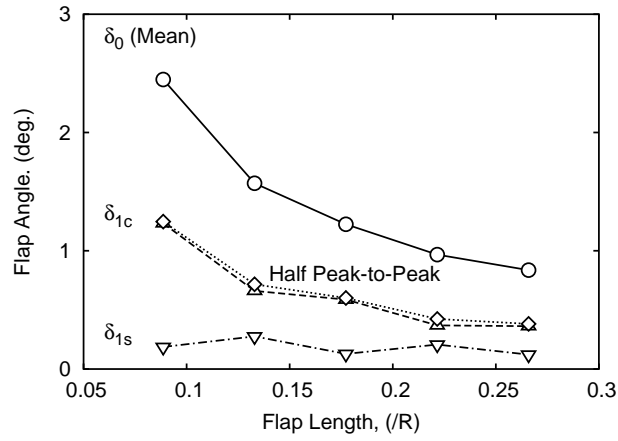


(a) Trailing-edge flap angle

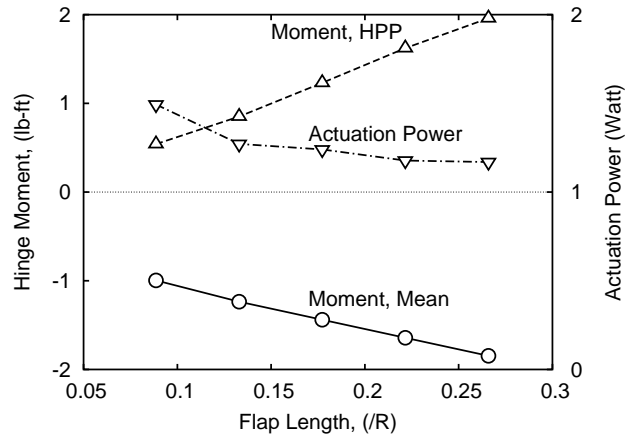


(b) Flap hinge moment and actuation power

Figure 9: Effect of flap spanwise location on flap deflection and actuation requirement (blade pitch index angle of  $18^\circ$ , flap length of  $18\%R$ ,  $\nu_\theta = 2.1/rev$ ,  $\mu = 0.30$ ).



(a) Trailing-edge flap angle



(b) Flap hinge moment and actuation power

Figure 10: Effect of flap length on flap deflection and actuation requirement (blade pitch index angle of  $18^\circ$ , flap middle section located at  $83\%R$ ,  $\nu_\theta = 2.1/rev$ ,  $\mu = 0.30$ ).

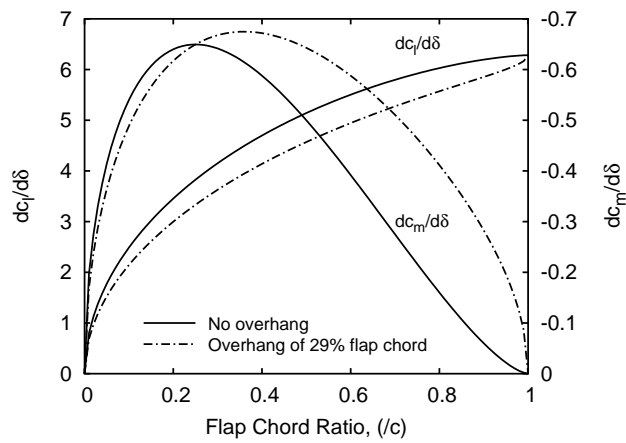
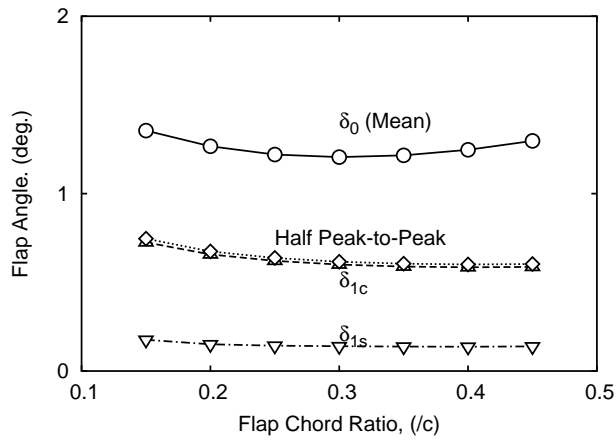
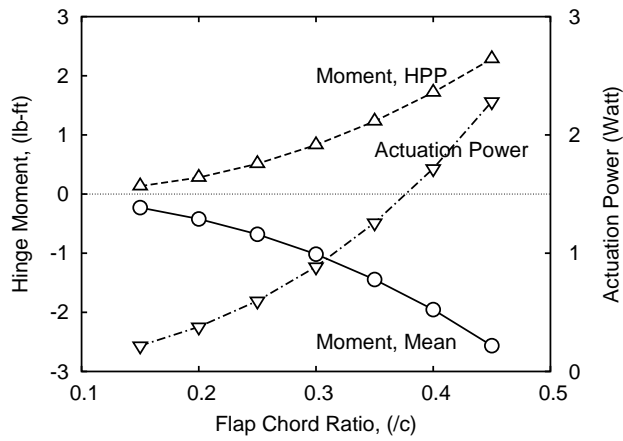


Figure 11: Theoretical lift and pitching moment characteristics of plain trailing-edge flaps

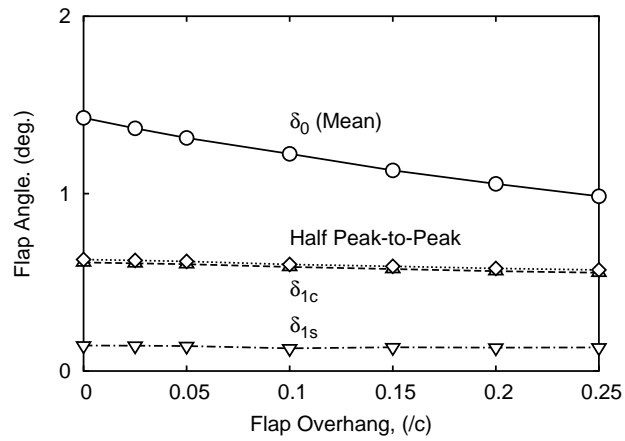


(a) Trailing-edge flap angle

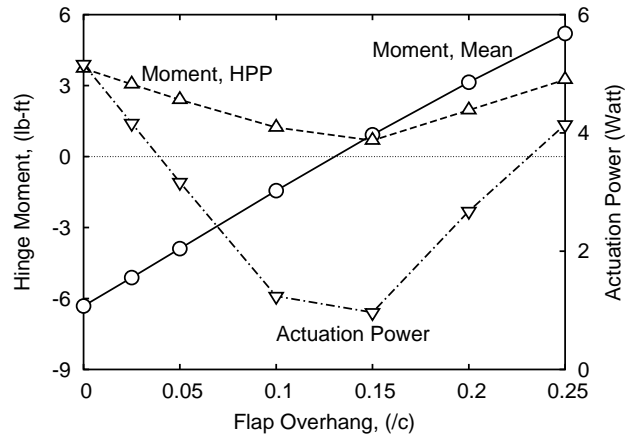


(b) Flap hinge moment and actuation power

Figure 12: Effect of flap chord ratio on flap deflection and actuation requirement (blade pitch index angle of  $18^\circ$ , flap overhang of 29% flap chord,  $\nu_\theta = 2.1/rev$ ,  $\mu = 0.30$ ).

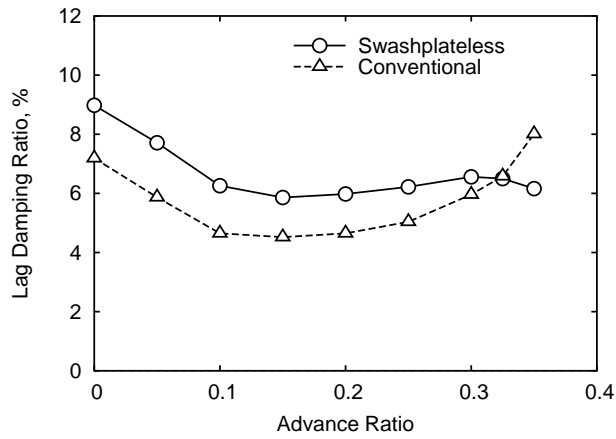


(a) Trailing-edge flap angle

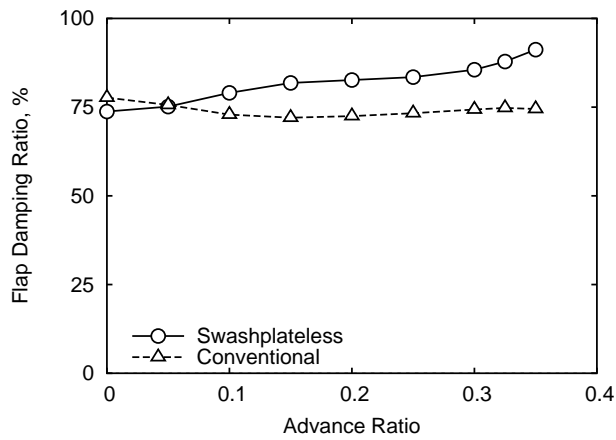


(b) Flap hinge moment and actuation power

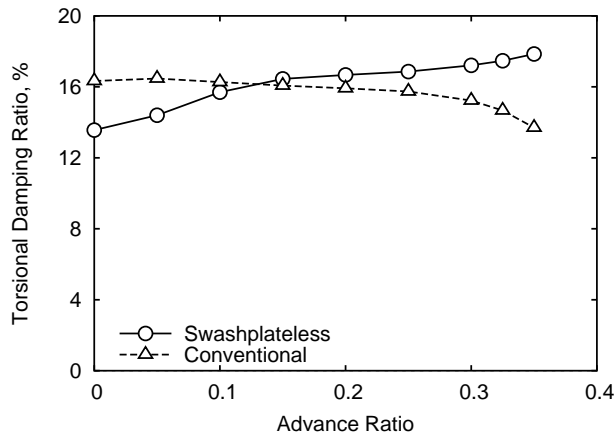
Figure 13: Effect of flap overhang on flap deflection and actuation requirement (blade pitch index angle of  $18^\circ$ , flap chord of  $0.35c$ ,  $\nu_\theta = 2.1/rev$ ,  $\mu = 0.30$ ).



(a) Blade lag damping

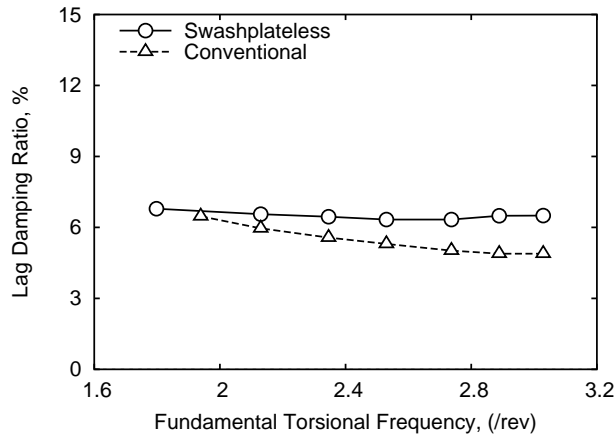


(b) Blade flap damping

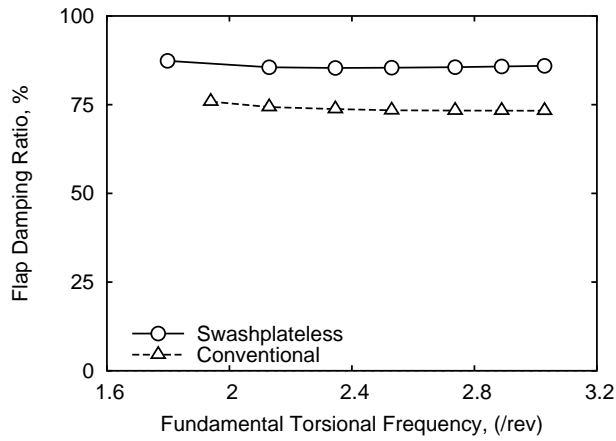


(c) Blade torsional damping

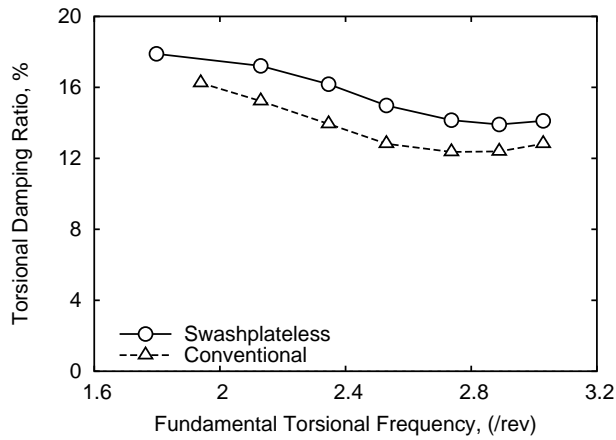
Figure 14: Comparison of blade stability for a swashplateless and conventional rotor at different forward speeds (blade pitch index angle of  $18^\circ$ ,  $\nu_\theta = 2.1/rev$ ).



(a) Blade lag damping



(b) Blade flap damping



(c) Blade torsional damping

Figure 15: Comparison of blade stability for a swashplateless and conventional rotor with various blade torsional frequencies (blade pitch index angle of  $18^\circ$ ,  $\mu = 0.30$ ).

## List of Figures

1	Trailing-edge flap with aerodynamic balance (nose overhang) . . . . .	22
2	Blade pitch indexing . . . . .	23
3	Trailing-edge flap deflection, blade pitch angle, and actuation requirement of swashplateless rotor at different forward speeds (blade pitch index angle of $18^\circ$ , $C_T/\sigma = 0.075$ , $\nu_\theta = 2.1/rev$ ). HPP: Half Peak-to-Peak . . . . .	24
4	Variation of blade torsion frequency with root spring stiffness and blade torsional stiffness distribution. . . . .	25
5	Effect of blade root spring stiffness and blade torsional stiffness on blade pitch and twist ( $\mu = 0.30$ ). . . . .	26
6	Effect of blade index angle on flap deflection, blade pitch angle, and flap actuation requirement ( $\nu_\theta = 2.1/rev$ , $\mu = 0.30$ ). HPP: Half Peak-to-Peak . . . . .	27
7	Effect of blade root spring stiffness on flap deflection, blade pitch angle, and flap actuation requirement (baseline blade torsional stiffness distribution, blade index angle of $18^\circ$ , $\mu = 0.30$ ). . . . .	28
8	Effect of blade torsional stiffness distribution on flap deflection, blade pitch angle, and flap actuation requirement (blade root spring stiffness of 119 lb/in, blade pitch index angle of $18^\circ$ , $\mu = 0.30$ ). . . . .	29
9	Effect of flap spanwise location on flap deflection and actuation requirement (blade pitch index angle of $18^\circ$ , flap length of $18\%R$ , $\nu_\theta = 2.1/rev$ , $\mu = 0.30$ ). . . . .	30
10	Effect of flap length on flap deflection and actuation requirement (blade pitch index angle of $18^\circ$ , flap middle section located at $83\%R$ , $\nu_\theta = 2.1/rev$ , $\mu = 0.30$ ). . . . .	31
11	Theoretical lift and pitching moment characteristics of plain trailing-edge flaps . . . . .	32
12	Effect of flap chord ratio on flap deflection and actuation requirement (blade pitch index angle of $18^\circ$ , flap overhang of 29% flap chord, $\nu_\theta = 2.1/rev$ , $\mu = 0.30$ ). . . . .	33
13	Effect of flap overhang on flap deflection and actuation requirement (blade pitch index angle of $18^\circ$ , flap chord of $0.35c$ , $\nu_\theta = 2.1/rev$ , $\mu = 0.30$ ). . . . .	34

14	Comparison of blade stability for a swashplateless and conventional rotor at different forward speeds (blade pitch index angle of $18^\circ$ , $\nu_\theta = 2.1/rev$ ). . . . .	35
15	Comparison of blade stability for a swashplateless and conventional rotor with various blade torsional frequencies (blade pitch index angle of $18^\circ$ , $\mu = 0.30$ ). . . . .	36

## List of Tables

1	Baseline Rotor (MD-900) and Flap Properties . . . . .	20
2	Prescribed shaft angles in different forward speeds. (Positive is tilt forward) . . . .	21